ChemComm

FEATURE ARTICLE

View Article Online
View Journal | View Issue

Cite this: *Chem. Commun.*, 2018, **54**, 13773

Progress towards creating optically addressable molecular qubits

Majed S. Fataftah and Danna E. Freedman *

Received 4th October 2018,
Accepted 14th November 2018

DOI: 10.1039/c8cc07939k

rsc.li/chemcomm

The emerging field of quantum information science promises to transform a diverse range of scientific fields, ranging from computation to sensing and metrology. The interdisciplinary scientific community laid the groundwork for the next generation of quantum technologies through key advances in understanding the fundamental unit of quantum information science, the qubit. Electronic spin is a promising platform for qubits, demonstrating suitably long coherence times, optical initialization, and single spin addressability. Herein, we discuss recent accomplishments and future progress from our group targeted at imbuing transition metal complexes with the aforementioned properties, creating a pathway to fusing spatial precision with long coherence times. A strong emphasis of this feature article is progressing towards single spin measurements *via* a chemical approach for imbuing molecular qubits with an optically-induced spin polarization mechanism.

Introduction

Quantum information science (QIS) is an emerging paradigm with the potential to revolutionize a diverse range of scientific fields.[1–3] Quantum bits, or qubits are the core of any QIS system and can be any quantum two-level system.[4] Qubits differ from their classical analogues through their ability to be placed into any superposition of the two quantum levels. This lends inherent parallelism to the computation paradigm, allowing the quantum system to sample multiple solutions simultaneously. The theorized computational enhancement for quantum computing may enable the solution of currently intractable computational problems, with applications ranging from structural biology to the simulation of quantum phenomena.[5,6]

Electronic spin-based qubits offer significant promise for the implementation of QIS. With electronic spin based qubits, computation is predicated on manipulating the electronic spin between its pair of M_S levels (*e.g.* $M_S = \pm 1/2$) using pulsed microwave irradiation.[7,8] Within the class of electronic spin qubits, paramagnetic molecular species are an attractive platform.[9–11] These highly tuneable species enable us to exploit our chemical toolkit to impact quantum properties. More importantly, they provide a pathway towards acquiring fundamental knowledge regarding the chemical design principles necessary to optimize and tailor the properties of the electronic spin towards a specific device architecture or application.

A specific set of criteria was formalized almost two decades ago by DiVincenzo to realize a viable qubit within any platform.[12] The DiVincenzo criteria require a qubit to: (1) be a well-defined quantum two-level system; (2) exhibit long superposition lifetimes; (3) satisfy a universal set of quantum operations; (4) be readily initialized; and (5) feature a readout mechanism for the quantum state of the qubit. As described above, electronic spin-based qubits offer a pathway for each of the above requirements. Any pair of well-defined M_S states (*e.g.* $M_S = \pm 1/2$ within $S = 1/2$ or $M_S = 0$ and -1 within $S = 1$) can serve as a qubit if it can be manipulated into a superposition state using pulsed microwaves. Recent studies of molecular species demonstrated T_2 times, or coherence times, exceeding the requisite threshold for this figure of merit, $\sim$100 μs.[13] Electronic spin qubits also offer pathways for multiple qubits to be entangled, a prerequisite for performing complex gate operations.[14] The final two criteria, initialization and readout pose a challenge, but there are numerous approaches to read out a single electronic spin-based qubit. Notably, using defects within diamond or silicon carbide it is possible to engender an optically addressable system.[15–18] These systems offer a pathway forward for molecular qubits.

For an illustrative example of a defect-based electronic spin qubit, we will focus on nitrogen vacancy centers (NVCs) in diamond. These defects combine long coherence times with an electronic structure that facilitates optically induced spin polarization for qubit initialization.[19] Crucially, these centers are emissive with spin-dependent fluorescence which permits optical readout of their spin dynamics. The facile ability to optically read out qubits enables single-qubit measurements on NVCs in diamond, and other analogous systems.[20] Defect-based systems are incredibly powerful, yet currently suffer from a lack of spatial precision. Imbuing optically addressable qubits with

Department of Chemistry, Northwestern University, Evanston, IL 60208, USA. E-mail: danna.freedman@northwestern.edu

spatial precision would fuse single qubit readout capabilities with the atomic precision required to execute quantum operations. Molecular qubits offer a pathway to mimic these properties *via* ligand field design.

Herein, we will describe our initial synthetic efforts to design molecular qubit candidates with the same key features as defect-based systems. We proceeded in two parallel directions, the first of which was to create long-lived qubits, by understanding the factors that contribute to decoherence, and designing new systems based upon that knowledge. Within a second approach, we are pursuing optically addressable molecular systems. We will briefly review our prior research on creating design principles to achieve long coherence times and devote the majority of the article to our research in progress on imbuing molecules with the same electronic structure as NVCs.

The key figure of merit that dictates a qubits viability is its coherence time (T_2), the lifetime of the superposition state.[8] One of the advantages of electronic spin-based qubits is their capacity to interact with other spins over long distances owing to their high sensitivity to their chemical environment. However, this sensitivity to the nuclear spin-laden environment leads to the rapid collapse of their superposition states in a process known as decoherence. Nuclear spins are an endemic source of magnetic noise, generated by the rapid, random flipping of their spins.[21] The oft-cited minimum T_2 is 100 μs, and until recently, most molecular qubits exhibited T_2 times below ~10 μs. To increase coherence time, we focused on nuclear spin-free ligand designs. These ligands are composed of only elements with very low abundance spin-active nuclei, such as carbon, oxygen, and sulphur, from which a variety of chelating ligands, and their metal complexes could be synthesized, such as $[V(C_8S_8)_3]^{2-}$, and $[Fe(C_5O_5)_3]^{3-}$, $[Cr(C_3S_5)_2]^{3-}$.[22–24] While these compounds displayed promise, their T_2's remained modest at best, likely owing to the nuclear spin bath of the surrounding chemical matrix. By employing the nuclear spin-free solvent, CS_2 we increased T_2 to 0.7 ms, comparable to coherence times in NVCs (Fig. 1a).[16] To examine whether this was a universal design principle, we probed a series of $S = 1/2$ vanadyl complexes dissolved in the nuclear spin-free solvent, SO_2, and demonstrated T_2's exceeding the requisite 100 μs threshold,[25] thereby establishing the viability of molecular qubits.[26,27]

While nuclear spin free systems are appealing, to access a broader range of synthetic tools, it would be ideal to understand how to incorporate nuclear spin into molecular qubits while subduing their detrimental impact on T_2. Here, we modulated the distance between an electronic spin and nuclear spin and studied their T_2 properties. This was achieved by designing and synthesizing a series of vanadyl complexes with a nuclear spin-laden propyl moiety placed at variable distances from the vanadyl spin centre, connected through a variable nuclear spin-free carbon–sulphur binary bridge (Fig. 1b).[28,29] These four complexes feature vanadyl–proton distances ranging from 4.0 to 12.6 Å, designed with the aim at elucidating the position of the spin-diffusion barrier, a critical radius separating two regimes. Inside the spin-diffusion barrier nuclear spins are so strongly coupled to the electronic spin it restricts their spin

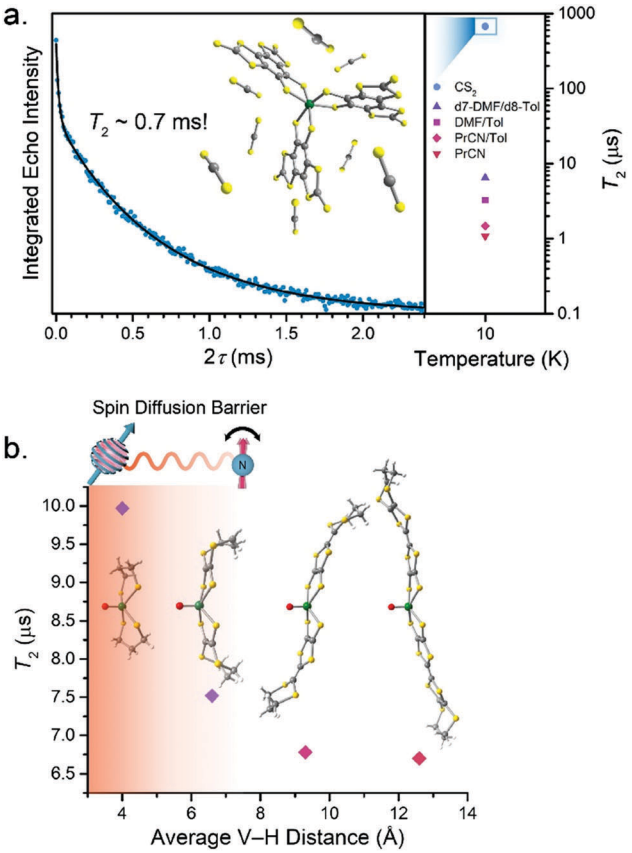

Fig. 1 Exploration of design principles governing coherence times in molecular electronic spin-based qubits. (a) Millisecond coherence time in $[V(C_8S_8)_3]^{2-}$ in CS_2, with solvent dependence of T_2 across a series of glassing solvents. (b) Dependence of T_2 on metal–proton distance in a series of vanadyl dithiolate complexes, highlighting the spin-diffusion barrier.

flip-flops that induce decoherence. Beyond this radius, spins readily undergo flip-flops on the experimental timescale and are the major source of decoherence.[30] Inspection of their low-temperature T_2 times plotted as a function of M–H distance clearly points to a critical distance beyond which T_2 rapidly decreases. These results suggest a barrier position between 4.0 and 6.6 Å for this system. The small decrease in T_2 from 9.2 to 12.6 Å suggests nuclear spins beyond this distance do not contribute considerably to decoherence. This is rationalized by the insensitivity of the electronic spin to the local fluctuating magnetic fields of nuclei too far away, which thereby do not contribute to decoherence. These results suggest a synthetic pathway forward.

We also approached increasing coherence time in molecular systems by seeking to insulate qubits from magnetic noise. Here, we employed clock transitions which feature an avoided level-crossing where the local slope of each spin sublevel (df/dB) is zero (Fig. 2a). The zero slope renders the electronic spin insensitive to local fluctuations of the magnetic field. Prior to our work there were two elegant proof-of-concept systems demonstrating this effect, a Bi-doped silicon material, and a Ho^{3+}-based polyoxometalate $[Ho(W_5O_{18})_2]^{9-}$.[31–33]

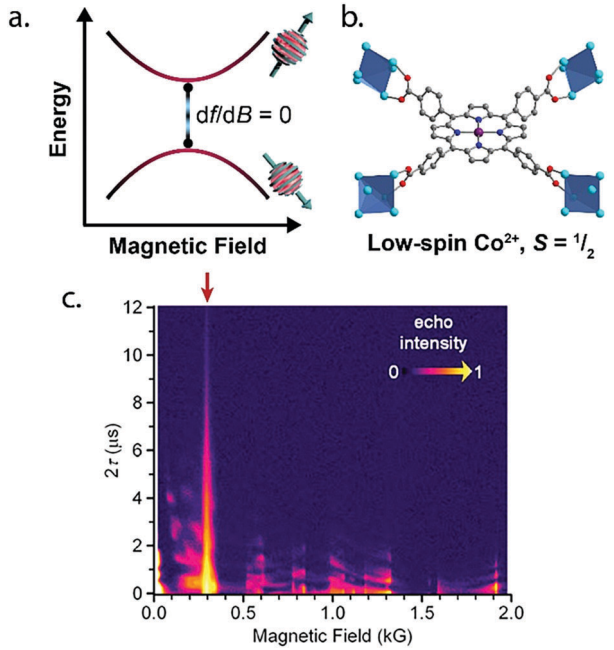

Fig. 2 (a) Qualitative Zeeman energy level diagram illustrating the level mixing between two M_S states, leading to an avoided level crossing, or clock transition. (b) Molecular structure of the Co^{2+} metalated porphyrin core within PCN-224 as determined by single-crystal X-ray diffraction. Purple, blue, red, and grey spheres represent Co, N, O, and C atoms, respectively, while the blue octahedra represent the Zr^{4+} clusters. (c) Contour plot of the field-dependence of T_2 in Co^{2+}-PCN-224 collected at 3.66 GHz, and 15 K, illustrating the dramatically elongated T_2 at the clock transition at ~0.3 kG.

Accessing spin transitions exhibiting an avoided level crossing requires a strong interaction mixing the two states, such as hyperfine interactions in the former example, and crystal field splitting in the latter. To bring this concept into coordination chemistry, we sought to combine hyperfine coupling with an $S = 1/2$ centre. We selected Co^{2+} which offers a nearly isotopically pure $I = 7/2$ ground state, thereby enabling us to target both the clock transition and a regular Zeeman transition as an internal control. To ensure an $S = 1/2$ ground state, we employed a porphyrin-based system placing the Co^{2+} ion in a square planar geometry (Fig. 2b). In this geometry, strong s-d_{z^2} orbital mixing gives rise to $A_{\parallel}$ value exceeding 1 GHz. We sought to study these molecules embedded within metal–organic frameworks (MOF)s to study the impact of magnetically noisy environments on coherence times. The resultant T_2 values evaluated across a series of transitions in $Co_{0.07}/Zn_{0.93}$ diluted MOF, plotted in Fig. 2c, reveals a T_2 value of 12 μs at 0.3 kG, dramatically longer than the remainder of non-clock transitions examined. This is a promising approach accessing long coherence times in nuclear spin-loaded environments.

One key advantage of the MOF based system, described above, is the potential for framework chemistry to engender networks of spatially precise qubits. Yet, within the previous example, we had to use magnetically dilute networks, thereby obviating the key advantage of MOFs. We therefore sought to access a fully spin-concentrated framework. One key reason

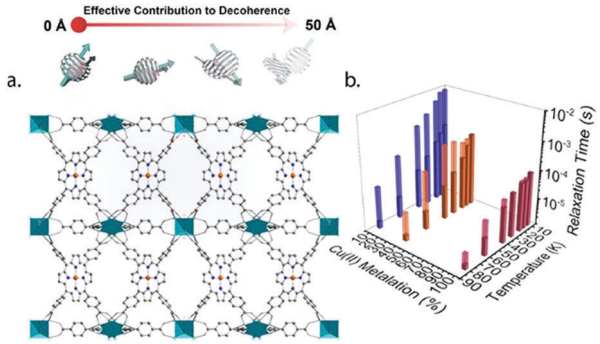

Fig. 3 (a) Crystal structure of $Cu_{1.0}$-PCN-224, highlighting the Zr-based polyhedral nodes, and the Cu^{2+}-porphyrin linkers. Top: Schematic illustrating the relative contribution of spins with variable distances, with negligible contributions to decoherence beyond 50 Å. (b) Plot of the ratio of T_1 (solid bars) to spectral diffusion (faded bars) at the three concentrations investigated (10%: purple, 40%: orange, 100%: red) across the temperature range of 10 to 80 K.

that a spin concentrated framework is relevant is that it allows us to understand spin–spin interactions based on a lattice with precisely reproducible qubit–qubit distances. We investigated the T_2 and T_1 properties of the Cu^{2+} porphyrin-based framework, Cu_x-PCN-224 presented in Fig. 3a. In this MOF, x was varied at values of 0.1, 0.4, and crucially, 1, yielding a fully concentrated array of $S = 1/2$ qubits.[34] Within the more dilute MOFs the remaining sites $(1 - x)$ were unmetalated porphyrin units. The materials were investigated in the temperature range of 10–80 K, yielding T_2 values ranging from 1 μs for $Cu_{0.1}$-PCN-224 to 50 ns for $Cu_{1.0}$-PCN-224. The major source of decoherence in this material arises from flipping electronic spins and electron–electron cross relaxation. This led us to conclude T_1 and electronic spin cross relaxation, or spectral diffusion, are limiting factors in ordered arrays of qubits. Modelling our T_2 data accounting for spin–spin dipolar interactions suggests electronic spins within a 50 Å radius are the major source of decoherence.[35] Furthermore, our analysis for T_1 across the concentration series highlights the prevalent role of spectral diffusion. The bar graph in Fig. 3b illustrates a hundred-fold increase in the relative ratio of spectral diffusion to T_1 with increasing spin concentration. The aggregate of these studies demonstrates a new set of design principles for the synthesis of arrays of qubits.

Pathways towards single qubit addressability

Ensemble studies are ideal for gaining fundamental insight into qubits, and for rapid screening of candidates. Thus far, molecular qubit experiments have been limited to ensemble measurements of molecules in solution, or in solid-state dilutions. Progressing towards true molecular implementations of QIS requires moving beyond ensemble measurements to single qubit measurements.[36]

Two promising routes towards single-molecule addressability are: (i) imbuing qubits with an optical read-out scheme; and

(ii) electrical detection *via* construction of single-molecule readout devices.[37] Single-molecule EPR readout requires extremely high sensitivity detection techniques. One highly successful approach is optically detected magnetic resonance (ODMR), which enables single-spin measurements of a nitrogen-vacancy centre in diamond.[20] An alternative approach relies on electrically detected magnetic resonance (EDMR). This technique utilizes a molecular junction, in which one molecule is sandwiched between two conductive electrodes, making contact through covalent chemical linkers. Its first proposed implementation was for a polyoxometalate molecular qubit,[38] and has been successfully extended to electrically controlling nuclear spins in the single-molecule magnet $TbPc_2$,[39] and to controlling electronic spins in endohedral fullerenes and solid-state systems.[40,41] The proposed implementation relies on tunnelling of an electric current through a single, paramagnetic molecule, and using spin transport selection rules to analyse the resulting spin character of the molecule.[42] A schematic of this device in drawn in Fig. 4, in which the molecular junction consists of a substrate, two electrodes, an electrical circuit, and the target molecule. A micro-magnet overlapping with one of the electrodes can act as both a spin injector to induce spin polarization, as well as a spin filter for magnetic resonance detection based on the spin valve effect.[43] Another micro-magnet incorporated in a microwave circuit generates the oscillating magnetic field needed to measure the EDMR effect.[44,45] This strategy towards single molecule measurements is a very attractive approach towards coupling molecular qubits with superconducting qubits, which benefit from their ease of fabrication using currently available technologies.[46]

An alternative approach towards accessing single qubit readout and initialization, which is the focus of the remaining discussion, is optical addressability. Specifically, we seek to achieve this by imbuing molecular candidates with mechanisms for qubit initialization and readout.[20] These mechanisms proceed through optically-induced spin polarization and photoluminescence readout of the spin quantum state.[47] This strategy has long been exploited in NVCs in diamond, divacancies in silicon carbide (SiC), and more recently Cr^{4+} impurities in gallium nitride (GaN).[48–50] Despite their varying optical, electronic, and

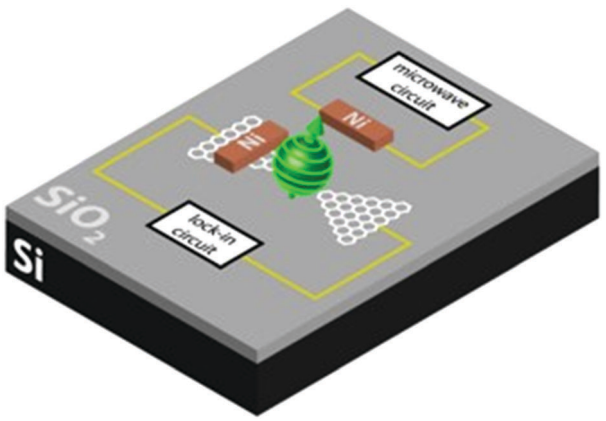

Fig. 4 Schematic of the molecular junction single-molecule EPR device described in the main text.

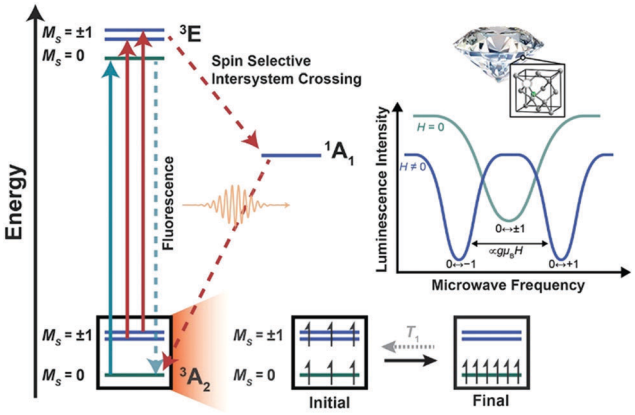

Fig. 5 Operative optically induced spin polarization mechanism for NVCs in diamond. This mechanism exploits spin-selective intersystem crossing to affect selective population of the $M_S = 0$ spin sublevel, and fluorescent readout of the spin quantum state.

structural properties, these defect sites all feature one common property: an $S = 1$ impurity featuring a spin-selective intersystem crossing (ISC) relaxation pathway that enables polarization of spins into a specific spin sublevel (M_S state).[51,52] This spin-selective ISC relaxation pathway is unique to non-Kramers spin systems, as it relies on the unique $M_S = 0$ state. For simplicity, the ensuing discussion will focus on NVCs in diamond as they are the most comprehensively studied and understood. This defect site exploits a spin-selective ISC relaxation pathway that polarizes the spins into the $M_S = 0$ state of the $^3A_2$ ground state. As illustrated in Fig. 5, this relaxation pathway directly relies on preferential ISC of the $M_S = \pm 1$ states within ^3E excited state to a lower energy singlet state ($^1A_1$), which then undergoes ISC to the $^3A_2$ ground state. Meanwhile, the $M_S = 0$ state within the ^3E state fluoresces back to the $M_S = 0$ state of the $^3A_2$ ground state. The selective ISC of the $M_S = \pm 1$ states within the ^3E state enables redistribution of populations within the ground state into the $M_S = 0$ state. This polarization pathway enables optical pumping of the first spin-allowed electronic transition, engendering a large spin polarization even at room temperature.[53] Furthermore, the photoluminescence is highly sensitive to the population of the $^3A_2$ $M_S = 0$ sublevel. The frequency-dependent integrated luminescence (Fig. 5) illustrates the decrease in emission upon resonant microwave excitation. This optical change can be utilized to read out the qubit state during microwave manipulation of the spin. Since optical change is used for readout, initial spin-polarization is a prerequisite for optical detection of spin dynamics, because without a known initial state it would not be possible to enable read out. These spin-dependent optical properties offer tremendous promise for quantum sensing applications, and enable single-qubit readout, thereby overcoming a key challenge for electronic spin-based qubits.

Progressing from individual qubits to multi-qubit arrays necessitates spatial control over qubits. Crucially, this is also a concern for sensing applications whereby it is important to precisely know the distance between a quantum sensor and

an analyte.[54–56] However, the major drawback for NVCs in diamond is the lack of spatial control over qubit location, whereby these defects are randomly generated throughout the diamond lattice.[57] This creates an impetus to translate their electronic structure into synthetically modular systems that enable spatial control over qubits. To enable that goal, we seek to imbue molecules with optical addressability, thereby uniting the optical addressability of NVCs with the atomic precision of molecular qubits. Herein, we discuss the design principles for synthesizing transition metal-based molecular qubit candidates with optically-induced spin polarization and readout pathways.

The first key design criterion is employing non-Kramers ions, specifically $S = 1$ electronic ground states, as the spin-selective ISC relaxation pathway requires the $M_S = 0$ state. Within this manifold, symmetry considerations are essential to obtain EPR addressable transitions. Frequently, $S = 1$ compounds are considered "EPR silent" owing to their large ground state axial zero-field splitting (D). This in turn prohibits manipulation of spins when D is much larger than the accessible microwave frequencies, and thus impedes our efforts to exert quantum control over the electronic spin. As zero-field splitting is a second order term incorporating orbital angular momentum, it depends heavily on spin–orbit coupling and low-lying excited states. Our two primary concerns are atomic number and orbital configuration, specifically the energetic separation between the pairs of d-orbitals comprising the $L = \pm1$ and ±2 sets [$L = \pm1$: xz, yz; $L = \pm2$: xy, $x^2 - y^2$]. Atomic number is important because spin–orbit coupling scales with Z_{eff}^4, thus excluding second- and third-row transition metals from consideration.[58]

Ligand field design can enable the creation of a system without unequal population of degenerate pairs of orbitals within the same $\pm L$ state.[59,60] Phrased differently, we can ensure no electron or hole resides jointly in two orbitals with the same value of $\pm L$. A degeneracy of this form is partially responsible for the generation of orbital angular momentum in species such as Ir^{4+} and Ru^{3+} and would skyrocket D to values not accessible with current microwave technology.[61] Considering all these design parameters, d^2 tetrahedral (T_d) and d^8 octahedral (O_h) compounds are most encouraging. In contrast, trigonal bipyramidal geometries are intriguing, as they enable fine-tuned control over D through prudent selection of the ligand field.[62]

Fulfilling the EPR addressability criterion thereby necessitates we focus on compounds of the first-row transition metals, such as V^{3+}, Cr^{4+}, Co^{1+}, and Ni^{2+}. Within the first-row transition metals, considerable efforts have focused on understanding the impact of symmetry and ligand field strength on D, with the focus on maximizing D for applications in single-molecule magnetism.[63] We aim to invert those design principles to access high-symmetry ligand field environments with small D-values. Isotropic electronic ground states (^{3}A symmetry) will be the first target. This prompts the design of compounds in trigonally symmetric ligand fields, whereby the two unpaired electrons occupy a set of two-degenerate orbitals, engendering ^{3}A ground states. T_d and O_h symmetries for d^2 and d^8 electron configurations, respectively, promise relatively small D-values. Herein, we will use three compounds previously reported in the literature to guide our discussion, specifically compounds of V^{3+}, Cr^{4+}, and Ni^{2+} which reside in trigonal ligand fields that yield ^{3}A ground states (Fig. 6).

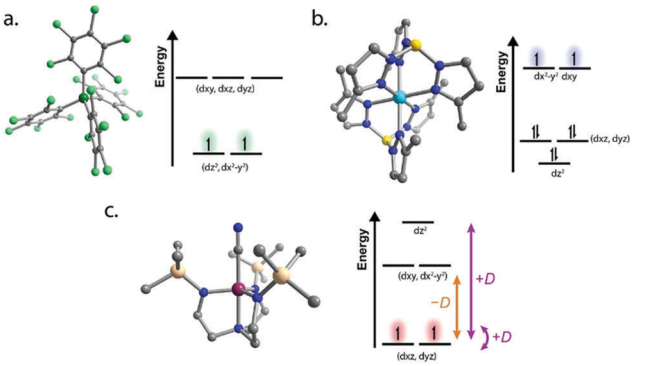

Fig. 6 Molecular structures of compounds **1–3** (a–c) as determined from single crystal X-ray diffraction studies, alongside their respective qualitative d-orbital splitting diagrams. Dark green, light blue, purple, light green, dark blue, yellow, beige, and grey spheres represent V, Ni, Cr, F, N, B, Si, and C atoms, respectively.

The first key step is enabling spin polarization, as it is a prerequisite is a prerequisite for optical readout. To enable the spin polarization mechanism described above, the lowest energy excited state must be a spin singlet state ($S = 0$). This is essential to facilitate ISC from the first spin-allowed triplet excited state. This necessitates the transition metal centre reside in a ligand field strong enough to destabilize the first triplet excited state above the singlet state. Inspection of the qualitative Tanabe–Sugano diagram based on the O_h d^8 (or T_d d^2) electron configurations reveals the singlet state (^{1}E) is approximately ligand field independent. In contrast, the first triplet state ($^3T_2$) increases linearly in energy with increasing ligand field strength. This is intuitive given the nature of the electronic transitions in question, as the singlet state only involves a spin-flip transition within the same orbital set. Within an ideal symmetry these assignments can be performed qualitatively, however as the symmetry deviates from idealized calculations are required to supplement assignments.

Using the new data described below, we will seek to illustrate the synthetic approach that can be harnessed to achieve the appropriate electronic structure. Within each molecular system described below, we demonstrate how tuning ligand field enables us to incorporate the design criteria described above, and what new design parameters we need to incorporate to translate this approach from materials to molecules.

Our investigation began with the V^{3+} compound, $[V(C_6Cl_5)_4]^-$ (**1**), which features the metal centre in a highly symmetric pseudo-T_d geometry.[64] To assess D, we collected the reduced magnetization data presented in Fig. 7a. Inspection of the magnetization data illustrates its highly isotropic ground state, with a saturation magnetization of 2 μ_B and near perfect overlay of the isofield lines. Simulation of the magnetization data with the Hamiltonian, $\hat{H} = D\hat{S}_z^2 + g_{iso}\mu_B\boldsymbol{SH}$, yields values of 0.4 cm^{-1} and 1.96 for D and g_{iso}, respectively.[65] It is worth noting the exact geometry about the V^{3+} centre in **1** is better approximated

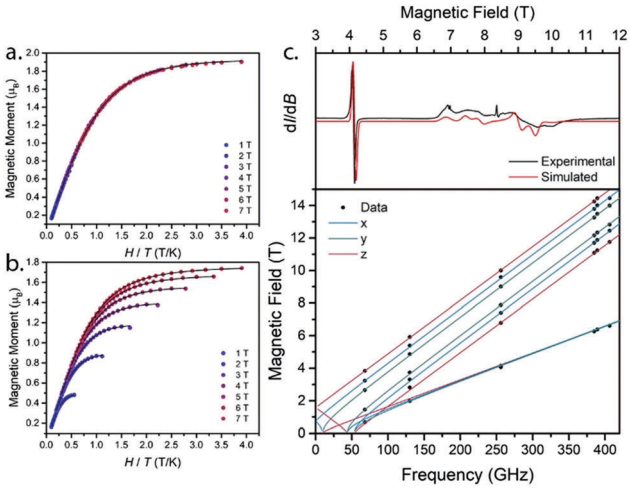

Fig. 7 (a) Reduced magnetization data for **1**, collected in the field and temperature range of 1–7 T and 1.8–10 K, respectively. (b) Reduced magnetization data for **3** collected under identical experimental conditions as in **1**. The different splitting of the isofield lines in a and b marks their different *D*-values. (c) 256 GHz experimental cw-EPR spectrum of **2** collected in the field range of 3–12 T and at 10 K (top). Frequency *versus* field dependence of the EPR transitions in **2**, showcasing the resonances observed across field and frequency, with best fits to data (solid lines).

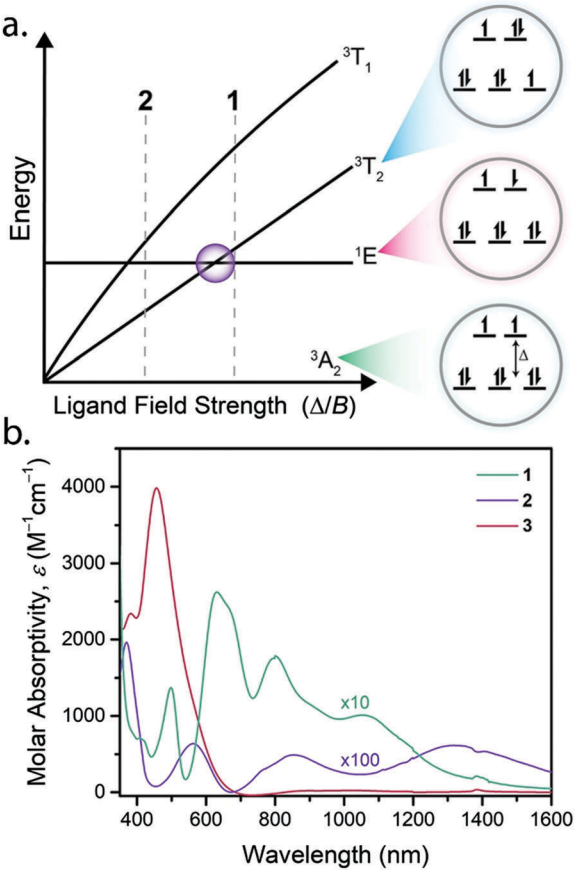

Fig. 8 (a) Qualitative Tanabe–Sugano diagram for a d^8 (O_h) system, illustrating how tuning the ligand field strength (Δ/B) changes the energy of the first allowed optical transition. (b) Electronic absorption spectrum of **1** (green), **2** (purple), and **3** (red). The data were collected in dichloromethane for **1** and **2**, and in 2-methyltetrahydrofuran for **3**. The spectra for **1** and **2** were magnified by factors of 10 and 100, respectively, for clarity.

as C_{2v} rather than T_d, further supporting a non-zero value of *D*. Regardless, these parameters establish accessible EPR transitions at conventional microwave frequencies. However, while the X-band cw-EPR spectrum could be collected on a microcrystalline sample of **1**, and was previously reported as well,[64] solutions of **1** in glassing solvents did not reveal a discernible signal. We attribute this discrepancy to inhomogeneity in *D* arising from fluxionality of the nonchelating pentachlorophenyl ligands. The effect is exacerbated by the magnitude of *D* being on par with X-band frequency ($h\nu \sim 0.32$ cm^{-1}). The lack of addressability violates DiVincenzo's first qubit design criterion, and adds another design parameter to our list, namely reducing ligand fluxionality to eliminate inhomogeneity in *D*. Alternately, we can pursue complexes with electronic structures that are impervious to structural variations, as was the case in the series of $[Fe(C_3S_5)_2]^{2-}$ previously reported.[66] Sterically encumbered ligands and rigid chelating ligands offer promise to suppress *D*-inhomogeneity.

We progressed from magnetic characterization to probing the spectral properties of **1** to determine its suitability as an optically addressable qubit in a solid-state matrix. A multitude of transitions are clearly identified in the wavelength range of 1400 nm to 400 nm for **1** and are readily assigned as d–d transitions given their low molar absorptivity (ε), as expected for Laporte allowed transitions (Fig. 8b). The dark forest green compound, **1**, features transitions at 1100 nm and 800 nm which correspond to transitions from the $^3A_2$ ground state to the $^3T_2$ excited state that splits under reduced symmetry, as expected given the distortion form ideal T_d to C_{2v}. The higher lying transitions at 600 and 480 nm are assigned to the split $^3T_2$ and higher lying $^3T_1$ states.[67] Ligand field strength is parameterized by Δ/B when using a Tanabe–Sugano diagram, where Δ and *B* are the crystal field splitting and Racah parameters, respectively. Hence, assignment of the d–d transitions permits determination of whether the ^1E state is the lowest energy excited state (Fig. 8a). These assignments permit determination of an approximate Δ/B ratio of 1.79, just past the requisite threshold of 1.68 highlighted in Fig. 8a. Thus, our analysis nominates **1** as a candidate to explore spin-dependent ISC and spin polarization. However, investigation of the compound by fluorimetry in 2-methyltetrahydrofuran at 77 K revealed no emissive features in the visible to near-IR energy range, precluding optical readout and identification of an ISC event. A potential culprit for the lack of emission is back-ISC, a phenomenon previously observed in Cr^{3+} compounds near the ISC cross-over point highlighted in Fig. 8a.[68] Future investigation of spin-polarization effects in **1** by transient EPR may provide insight into initialization.

Pseudo-octahedral complexes of Ni^{2+} are promising to access $S = 1$ complexes that can be addressed by current microwave frequencies. The near octahedral geometry surrounding the Ni^{2+} centre should enforce an isotropic magnetic ground state and yield relatively small values of *D*. We chose to investigate

the homoleptic methyl-substituted trispyrazolylborate complex of Ni^{2+}, $^{Me}Tp_2Ni$ (**2**), for two reasons.[69] First, an analogous octahedral hexakis-pyrazolyl Ni^{2+} complex, $[Pz_6Ni](ClO_4)_2$, was previously reported to possess a *D*-value of 0.07 cm^{-1} and negligible rhombicity.[70] Second, restricting the pyrazole ligands in a chelating ligand would suppress the influence of *D*-inhomogeneity. We investigated this complex by magnetometry and high-field, variable frequency EPR measurements. As seen in the top of Fig. 7c, the 256 GHz EPR spectrum collected at 10 K reveals many transitions that can be tracked across several microwave frequencies. These transitions are plotted as a function of field and frequency in the bottom of Fig. 7c. Global fitting of these transitions yield the following parameters: $D = -1.61$ cm^{-1}, $E = 0.16$ cm^{-1}, and *g*-values of 2.15, 2.155, 2.169 for g_x, g_y, and g_z, respectively. The 256 GHz cw spectrum was simulated using these parameters and reproduces the spectrum well at every frequency of measurement. The increase in *D* and rhombicity (*E*/*D*) in **2** is the product of descent in symmetry away from O_h towards D_{3d} owing to the chelating nature of ^{Me}Tp and the methyl group substituents. The relatively small *D*-value and nonzero *E*-value engender an accessible low-field transition that permits addressability of **2** by both X- (10 GHz) and Q-band (35 GHz). Thus, **2** can be addressed by EPR spectroscopy and is a promising candidate to explore the coherent spin properties in a $S = 1$ compound.

In contrast, analysis of the extremely low ε transitions of **2**, a very pale blue compound, reveals its ligand field is too weak to destabilize the first triplet excited state relative to the singlet state (Fig. 8b). The transitions at 1360, 850, and 570 nm are assigned as transitions from the $^3A_2$ ground state to the $^3T_2$, $^3T_1$ (^3F) and $^3T_1$ (^3P) excited states. These band assignments yield a Δ/B ratio of approximately 1.2, and is in close agreement with previously reported pyrazole and imidazole hexa-chelate complexes of Ni^{2+}.[71] This asserts **2** is an unsuitable candidate for the desired spin-polarization mechanism. Additionally, no emissive features in the visible range were identified for **2**. Irrespective of their ligand field strengths, both **1** and **2** feature exclusively d–d transitions in the visible-NIR range. These transitions possess very small ε-values, in the range of 100–300 for **1** and 5–20 for **2**, as expected for d–d transitions in pseudo-T_d and pseudo-O_h ligand field environments, respectively.[72] This must be circumvented if we are to access single-molecule studies, urging us to pursue charge transfer transitions.

Considering our new design parameter of chelating ligands, and the need for larger ε-values, we sought to explore the magnetic and optical properties of the Cr^{4+} compound, ^{TMS}trenCrCN (**3**).[73] Fig. 6c illustrates the trigonal bipyramidal geometry surrounding the Cr^{4+} ion, coordinated by three equatorial silylamide donors, along with an apical amine and cyanide donor occupying the axial positions. The scarcity of stable, crystallographically isolable Cr^{4+} compounds, and the even rarer reports of their magnetic properties urged us to investigate the magnetic properties of **3**.[74,75] The reduced magnetization of **3** presented in Fig. 7b reveals notable splitting between the isofield lines. This suggests the presence of substantial *D* and is supported by simulation of the data with the Hamiltonian, $\hat{H} = D\hat{S}_z^2 + (g_\parallel + g_\perp)\mu_B \boldsymbol{SH}$, which yielded a *D*-value of 4.8 cm^{-1}, and *g*-values of 1.96 and 1.98 for $g_\parallel$ and $g_\perp$, respectively. The substantial magnitude of *D* in **3** is unsurprising given its axial coordination environment, and clearly necessitates high frequency EPR (W-band, $\sim$95 GHz) to address any potential transitions and probe its qubit properties. More importantly, the C_{3v} symmetry of **3** provides us with a tunable ligand platform to exert synthetic control over *D*. Specifically, modification of the silyl substituents enables direct tuning of the (d_{xy}, $d_{x^2-y^2}$) antibonding orbital set which yields a negative contribution to *D* (Fig. 6c). Meanwhile substitution of the axial cyanide ligand allows us to tune the d_{z^2} orbital, which provides a positive contribution to *D*.[62,76] Fine-tuning the energetics of the d-orbitals, and consequently the lowest lying electronic excited states provides a rational methodology to tune *D* to access transitions at a targeted EPR frequency.

Inspection of the electronic absorption spectrum of **3** displays one sole charge transfer transition at 450 nm (Fig. 8b). This transition has an ε-value orders of magnitude larger than **1** or **2**, and obscures observation of the relevant d–d transitions. While optimal for optical addressability, obscuring electronic transitions within the d-manifold complicates our analysis. Moreover, the strong deviation in ligand field from T_d or O_h symmetry expunges our predictive capacities using a Tanabe–Sugano diagram. Thus, it becomes imperative we rely on experimental spectroscopic techniques, in conjunction with theoretical calculations, to identify the singlet state. Notably, the relaxation pathway post d–d excitation *versus* charge-transfer excitation may be dramatically different, and may impact the resultant spin polarization.[77] Future experiments will rely heavily on ultrafast pump–probe and time-resolved photoluminescence spectroscopy to identify ISC events and emissive features to exploit for optical readout.[78,79]

The criteria outlined thus far outline a pathway to design EPR addressable molecular qubits that enable optically induced spin polarization. Beyond these considerations, direct measurement of spin polarization typically proceeds *via* optically-detected magnetic resonance (ODMR) spectroscopy. This necessitates installing both a spin polarization and optical readout mechanism in triplet compounds. These experiments are impeded by accessible microwave frequencies, typically operable in the range of 10–20 GHz. Barring successful design of $S = 1$ compounds with appropriate *D*-values, future experiments will depend upon performing high-frequency ODMR,[80] transient EPR, and high-field level anti-crossing experiments to monitor spin polarization.[81] These experiments will be crucial to explore spin-selective ISC in transition metal compounds, and to understand the impact of spin–orbit coupling on the excited state dynamics in these systems. These preliminary experiments will be the initial steps towards understanding the relaxation dynamics within the excited state manifold responsible for spin polarization and will inform future design criteria.

Conclusions

Molecular systems demonstrate significant promise towards understanding spin dynamics of candidate qubits. Progressing from proof-of-concept studies towards realization of QIS schemes

necessitates achieving single qubit read-out. Mimicking the electronic structure of NVCs in molecular systems offers a promising route toward achieving this goal through optical addressability. Engendering the same electronic structure within a molecular system is a vital new challenge for inorganic chemistry. Creating these systems builds on decades of understanding of manipulation of ligand fields to impact electronic structure of coordination compounds. In the foregoing discussion we outlined the initial steps towards this goal, and we envision qubits of this kind becoming a new synthetic target for inorganic chemists.

Progressing beyond the results described herein necessitates careful consideration of the design principles enumerated above. Specifically, a focus on modular $S = 1$ compounds with strong field, chelating ligands should enable tuning of both the ground state and excited state manifolds. Synthetic modularity of the ligand field will enable fine-tuning of D-values that will enable EPR addressability below 20 GHz. Additionally, we envision designing compounds that feature metal to ligand charge transfer transitions may enable radiative relaxation that is competitive with ISC events, both essential ingredients towards accessing optical addressability in molecular qubit candidates. Ultimately, uniting our design criteria for enhancing T_2 within molecular qubits with the above ligand field considerations for optically addressable systems will enable the next generation of qubits: spatially precise and optically addressable.

Conflicts of interest

There are no conflicts to declare.

Acknowledgements

We thank Mr Scott Coste, Mr Dan Laorenza, Prof. Joseph Zadrozny, Dr Andrew Ozarowski, Dr Matt Krzyaniak, Dr Ryan Young, and Mr Brian Phelan for discussions and scientific insight. This work was supported by Northwestern University, the State of Illinois, and the National Science Foundation CAREER Award No. CHE-1455017. A portion of this work was performed at the National High Magnetic Field Laboratory, which is supported by the National Science Foundation Cooperative Agreement No. DMR-1644779 and the State of Florida.

Notes and references

1 S. Lloyd, *Science*, 1996, **273**, 1073.
2 J. Stolze and D. Suter, *Quantum Computing: A Short Course from Theory to Experiment*, Wiley-VCH Verlag GmBJ & Co. KGaA, Weinheim, 2008.
3 M. A. Nielsen and I. L. Chuang, *Quantum Information and Quantum Computation*, Cambridge University Press, Cambridge, 2010.
4 T. D. Ladd, F. Jelezko, R. Laflamme, Y. Nakamura, C. Monroe and J. L. O'Brien, *Nature*, 2010, **464**, 45.
5 N. Lambert, Y. N. Chen, Y. C. Cheng, C. M. Li, G. Y. Chen and F. Nori, *Nat. Phys.*, 2012, **9**, 10.
6 T. H. Johnson, S. R. Clark and D. Jaksch, *EPJ Quantum Technology*, 2014, **1**, 10.
7 A. Ardavan and S. J. Blundell, *J. Mater. Chem.*, 2009, **19**, 1754.
8 A. Schweiger and G. Jeschke, *Principles of Pulse Electron Paramagnetic Resonance*, Oxford University Press, New York, 2001.
9 F. Troiani and M. Affronte, *Chem. Soc. Rev.*, 2011, **40**, 3119.
10 G. Aromí, D. Aguilà, P. Gamez, F. Luis and O. Roubeau, *Chem. Soc. Rev.*, 2012, **41**, 537.
11 M. J. Graham, J. M. Zadrozny, M. S. Fataftah and D. E. Freedman, *Chem. Mater.*, 2017, **29**, 1885–1897.
12 D. P. DiVincenzo, *Fortschr. Phys.*, 2000, **48**, 771.
13 J. M. Zadrozny, J. Niklas, O. G. Poluektov and D. E. Freedman, *ACS Cent. Sci.*, 2015, **1**, 488.
14 F. Dolde, I. Jakobi, B. Naydenov, N. Zhao, S. Pezzagna, C. Trautmann, J. Meijer, P. Neumann, F. Jelezko and J. Wrachtrup, *Nat. Phys.*, 2013, **9**, 139.
15 M. W. Doherty, N. B. Manson, P. Delaney, F. Jelezko, J. Wrachtrup and L. C. L. Hollenberg, *Phys. Rep.*, 2013, **528**, 1.
16 W. F. Koehl, B. B. Buckley, F. J. Heremans, G. Calusine and D. D. Awschalom, *Nature*, 2011, **479**, 84.
17 M. Widmann, S. Y. Lee, T. Rendler, N. T. Son, H. Fedder, S. Paik, L. P. Yang, N. Zhao, S. Yang, I. Booker, A. Denisenko, M. Jamali, S. A. Momenzadeh, I. Gerhardt, T. Ohshima, A. Gali, E. Janzén and J. Wrachtrup, *Nat. Mater.*, 2014, **14**, 164.
18 D. J. Christle, A. L. Falk, P. Andrich, P. V. Klimov, J. U. Hassan, N. T. Son, E. Janzén, T. Ohshima and D. D. Awschalom, *Nat. Mater.*, 2014, **14**, 160.
19 V. V. Dobrovitski, G. D. Fuchs, A. L. Falk, C. Santori and D. D. Awschalom, *Annu. Rev. Condens. Matter Phys.*, 2013, **4**, 23.
20 F. Jelezko, T. Gaebel, I. Popa, A. Gruber and J. Wrachtrup, *Phys. Rev. Lett.*, 2004, **92**, 076401.
21 S. Takahashi, I. S. Tupitsyn, J. van Tol, C. C. Beedle, D. N. Hendrickson and P. C. E. Stamp, *Nature*, 2011, **476**, 76.
22 J. M. Zadrozny, J. Niklas, O. G. Poluektov and D. E. Freedman, *J. Am. Chem. Soc.*, 2014, **136**, 15841.
23 J. M. Zadrozny and D. E. Freedman, *Inorg. Chem.*, 2015, **54**, 12027.
24 M. S. Fataftah, J. M. Zadrozny, S. C. Coste, M. J. Graham, D. M. Rogers and D. E. Freedman, *J. Am. Chem. Soc.*, 2016, **138**, 1344.
25 C. J. Yu, M. J. Graham, J. M. Zadrozny, J. Niklas, M. Krzyaniak, M. R. Wasielewski, O. G. Poluektov and D. E. Freedman, *J. Am. Chem. Soc.*, 2016, **138**, 14678.
26 R. Sessoli, *ACS Cent. Sci.*, 2015, **1**, 473–474.
27 K. Bader, D. Dengler, S. Lenz, B. Endeward, S. D. Jiang, P. Neugebauer and J. van Slageren, *Nat. Commun.*, 2014, **5**, 5304.
28 M. J. Graham, C. J. Yu, M. D. Krzyaniak, M. R. Wasielewski and D. E. Freedman, *J. Am. Chem. Soc.*, 2017, **139**, 3196–3201.
29 M. J. Graham, M. D. Krzyaniak, M. R. Wasielewski and D. E. Freedman, *Inorg. Chem.*, 2017, **56**, 8106–8113.
30 S. S. Eaton and G. R. Eaton, *Distance measurements in biological systems by EPR*, Klewer Academic/Plenum Publishers, New York, 2002.
31 G. Wolfowicz, A. M. Tyryshkin, R. E. George, H. Riemann, N. V. Abrosimov, P. Becker, H. J. Pohl, M. L. W. Thewalt, S. A. Lyon and J. J. L. Morton, *Nat. Nanotechnol.*, 2013, **8**, 561.
32 G. Wolfowicz, S. Simmons, A. M. Tyryshkin, R. E. George, H. Riemann, N. V. Abrosimov, P. Becker, H. J. Pohl, S. A. Lyon, M. L. W. Thewalt and J. J. L. Morton, *Phys. Rev. B: Condens. Matter Mater. Phys.*, 2012, **86**, 245301.
33 M. Shiddiq, D. Komijani, Y. Duan, A. Gaita-Ariño, E. Coronado and S. Hill, *Nature*, 2016, **531**, 348.
34 C.-J. Yu, M. D. Krzyaniak, M. S. Fataftah, M. R. Wasielewski and D. E. Freedman, *Chem. Sci.*, 2019, DOI: 10.1039/C8SC04435J.
35 K. M. Salikhov, S. A. Dzuba and A. M. Raitsimring, *J. Magn. Reson.*, 1981, **42**, 255–276.
36 D. P. DiVincenzo, *J. Appl. Phys.*, 1999, **85**, 4785–4787.
37 J. J. L. Morton and P. Bertet, *J. Magn. Reson.*, 2018, **287**, 128–139.
38 J. Lehmann, A. Gaita-Ariño, E. Coronado and D. Loss, *Nat. Nanotechnol.*, 2007, **2**, 312.
39 S. Thiele, F. Balestro, R. Ballou, S. Klyatskaya, M. Ruben and W. Wernsdorfer, *Science*, 2014, **344**, 1135–1138.
40 W. Harneit, in *Endohedral Fullerenes: Electron Transfer and Spin*, ed. A. A. Popov, Springer International Publishing, Cham, 2017, pp. 297–324.
41 J. J. L. Morton and B. W. Lovett, *Annu. Rev. Condens. Matter Phys.*, 2011, **2**, 189–212.
42 L. Bogani and W. Wernsdorfer, *Nat. Mater.*, 2008, **7**, 179.
43 F. Zu, Z. Liu, K. Yao, G. Gao, H. Fu, S. Zhu, Y. Ni and L. Peng, *Sci. Rep.*, 2014, **4**, 4838.

44 C. Kloeffel and D. Loss, *Annu. Rev. Condens. Matter Phys.*, 2013, **4**, 51–81.
45 F. H. L. Koppens, C. Buizert, K. J. Tielrooij, I. T. Vink, K. C. Nowack, T. Meunier, L. P. Kouwenhoven and L. M. K. Vandersypen, *Nature*, 2006, **442**, 766.
46 D. Marcos, M. Wubs, J. M. Taylor, R. Aguado, M. D. Lukin and A. S. Sørensen, *Phys. Rev. Lett.*, 2010, **105**, 210501.
47 J. R. Weber, W. F. Koehl, J. B. Varley, A. Janotti, B. B. Buckley, C. G. Van de Walle and D. D. Awschalom, *Proc. Natl. Acad. Sci. U. S. A.*, 2010, **107**, 8513–8518.
48 A. L. Falk, B. B. Buckley, G. Calusine, W. F. Koehl, V. V. Dobrovitski, A. Politi, C. A. Zorman, P. X. L. Feng and D. D. Awschalom, *Nat. Commun.*, 2013, **4**, 1819.
49 W. F. Koehl, B. Diler, S. J. Whiteley, A. Bourassa, N. T. Son, E. Janzén and D. D. Awschalom, *Phys. Rev. B: Condens. Matter Mater. Phys.*, 2017, **95**, 035207.
50 W. F. Koehl, H. Seo, G. Galli and D. D. Awschalom, *MRS Bull.*, 2015, **40**, 1146–1153.
51 P. G. Baranov, I. V. Il'in, E. N. Mokhov, M. V. Muzafarova, S. B. Orlinskii and J. Schmidt, *J. Exp. Theor. Phys. Lett.*, 2005, **82**, 441–443.
52 N. T. Son, A. Ellison, B. Magnusson, M. F. MacMillan, W. M. Chen, B. Monemar and E. Janzén, *Phys. Lett.*, 1999, **86**, 4348–4353.
53 L. Robledo, H. Bernien, T. van der Sar and R. Hanson, *New J. Phys.*, 2011, **13**, 025013.
54 H. J. Mamin, M. Kim, M. H. Sherwood, C. T. Rettner, K. Ohno, D. D. Awschalom and D. Rugar, *Science*, 2013, **339**, 557–560.
55 R. Schirhagl, K. Chang, M. Loretz and C. L. Degen, *Annu. Rev. Phys. Chem.*, 2014, **65**, 83–105.
56 P. Maletinsky, S. Hong, M. S. Grinolds, B. Hausmann, M. D. Lukin, R. L. Walsworth, M. Loncar and A. Yacoby, *Nat. Nanotechnol.*, 2012, **7**, 320.
57 A. M. Edmonds, U. F. S. D'Haenens-Johansson, R. J. Cruddace, M. E. Newton, K. M. C. Fu, C. Santori, R. G. Beausoleil, D. J. Twitchen and M. L. Markham, *Phys. Rev. B: Condens. Matter Mater. Phys.*, 2012, **86**, 035201.
58 R. R. Schrock, S. W. Seidel, N. C. Mösch-Zanetti, D. A. Dobbs, K.-Y. Shih and W. M. Davis, *Organometallics*, 1997, **16**, 5195–5208.
59 D. Dai, H. Xiang and M.-H. Whangbo, *J. Comput. Chem.*, 2008, **29**, 2187–2209.
60 M. H. Whangbo, E. E. Gordon, H. Xiang, H. J. Koo and C. Lee, *Acc. Chem. Res.*, 2015, **48**, 3080.
61 K. S. Pedersen, J. Bendix, A. Tressaud, E. Durand, H. Weihe, Z. Salman, T. J. Morsing, D. N. Woodruff, Y. Lan, W. Wernsdorfer, C. Mathonière, S. Piligkos, S. I. Klokishner, S. Ostrovsky, K. Ollefs, F. Wilhelm, A. Rogalev and R. Clérac, *Nat. Commun.*, 2016, **7**, 12195.
62 B. Cahier, R. Maurice, H. Bolvin, T. Mallah and N. Guihéry, *Magnetochemistry*, 2016, **2**, 31.
63 R. A. Layfield, *Organometallics*, 2014, **33**, 1084–1099.
64 P. J. Alonso, J. Forniés, M. A. García-Monforte, A. Martín and B. Menjón, *Chem. Commun.*, 2001, 2138–2139.
65 R. T. Azuah, L. R. Kneller, Y. Qiu, P. L. W. Tregenna-Piggott, C. M. Brown, J. R. D. Copley and R. M. Dimeo, *J. Res. Natl. Inst. Stand. Technol.*, 2009, **114**, 341.
66 J. M. Zadrozny, S. M. Greer, S. Hill and D. E. Freedman, *Chem. Sci.*, 2016, **7**, 416–423.
67 P. J. Alonso, J. Forniés, M. A. García-Monforte, A. Martín and B. Menjón, *Chem. – Eur. J.*, 2005, **11**, 4713–4724.
68 S. Otto, M. Dorn, C. Förster, M. Bauer, M. Seitz and K. Heinze, *Coord. Chem. Rev.*, 2018, **359**, 102–111.
69 P. Cecchi, G. G. Lobbia, F. Marchetti, G. Valle and S. Calogero, *Polyhedron*, 1994, **13**, 2173–2178.
70 J. Reedijk and B. Nieuwenhuijse, *Recl. Trav. Chim. Pays-Bas*, 1972, **91**, 533–551.
71 J. Reedijk, *Recl. Trav. Chim. Pays-Bas*, 1969, **88**, 1451–1470.
72 B. N. Figgis and M. A. Hitchman, *Ligand Field Theory and Its Applications*, Wiley-VCH, New York, 2000.
73 Alexander C. Filippou, S. Schneider and B. Ziemer, *Eur. J. Inorg. Chem.*, 2002, 2928–2935.
74 P. J. Alonso, J. Forniés, M. A. García-Monforte, A. Martín, B. Menjón and C. Rillo, *Chem. – Eur. J.*, 2002, **8**, 4056–4065.
75 M. P. Marshak and D. G. Nocera, *Inorg. Chem.*, 2013, **52**, 1173–1175.
76 D. Schweinfurth, M. G. Sommer, M. Atanasov, S. Demeshko, S. Hohloch, F. Meyer, F. Neese and B. Sarkar, *J. Am. Chem. Soc.*, 2015, **137**, 1993.
77 S. Zerdane, L. Wilbraham, M. Cammarata, O. Iasco, E. Rivière, M. L. Boillot, I. Ciofini and E. Collet, *Chem. Sci.*, 2017, **8**, 4978–4986.
78 E. A. Juban and J. K. McCusker, *J. Am. Chem. Soc.*, 2005, **127**, 6857–6865.
79 J. N. Schrauben, K. L. Dillman, W. F. Beck and J. K. McCusker, *Chem. Sci.*, 2010, **1**, 405–410.
80 V. Stepanov, F. H. Cho, C. Abeywardana and S. Takahashi, *Appl. Phys. Lett.*, 2015, **106**, 063111.
81 R. J. Epstein, F. M. Mendoza, Y. K. Kato and D. D. Awschalom, *Nat. Phys.*, 2005, **1**, 94.